

Differentiable Logical Programming for Quantum Circuit Discovery and Optimization

Antonin Sulc

Lawrence Berkeley National Laboratory, Berkeley, California 94720, USA

Designing high-fidelity quantum circuits remains challenging, and current paradigms often depend on heuristic, fixed-ansatz structures or rule-based compilers that can be suboptimal or lack generality. We introduce a neuro-symbolic framework that reframes quantum circuit design as a differentiable logic programming problem. Our model represents a scaffold of potential quantum gates and parameterized operations as a set of learnable, continuous “truth values” or “switches,” $s \in [0, 1]^N$. These switches are optimized via standard gradient descent to satisfy a user-defined set of differentiable, logical axioms (e.g., correctness, simplicity, robustness). We provide a theoretical formulation bridging continuous logic (via T-norms) and unitary evolution (via geodesic interpolation), while addressing the barren plateau problem through biased initialization. We illustrate the approach on tasks including discovery of a 4-qubit Quantum Fourier Transform (QFT) from a scaffold of 21 candidate gates. We also report a hardware-aware adaptation experiment on the 133-qubit IBM Torino processor, where the method improved fidelity by 59.3 percentage points in a localized routing task while adapting to hardware failures.

1 Introduction

Quantum computation promises to solve problems considered intractable for classical computers, with applications spanning materials science and quantum chemistry, drug discovery, and complex optimization problems in areas such as fi-

Antonin Sulc: asulc@lbl.gov

nance and logistics [1, 2, 3, 4, 5]. However, realizing this potential depends on our ability to design and execute high-fidelity quantum circuits. In the current noisy intermediate-scale quantum (NISQ) era, this task is constrained; hardware is limited by gate error rates, coherence times, and qubit connectivity, placing a strong emphasis on circuit efficiency and robustness [6].

The central challenge is that finding an optimal quantum circuit for a given task is a notoriously difficult combinatorial search problem. Current approaches to circuit design, while powerful, face fundamental limitations.

Manual, human-derived circuits for canonical algorithms like the Quantum Fourier Transform (QFT) or Grover’s search are the product of significant ingenuity but are not generalizable to novel problems, such as simulating an arbitrary molecular Hamiltonian. Variational Quantum Algorithms (VQAs), the dominant NISQ paradigm [7, 8], typically rely on a pre-defined, fixed-structure “ansatz.” The performance of the entire algorithm is critically sensitive to this heuristic design choice. A poor ansatz can lead to an inability to express the solution state or suffer from barren plateaus, where training gradients vanish exponentially [9]. While adaptive methods like ADAPT-VQE [10] build an ansatz iteratively, they employ a greedy search that may not find a globally optimal structure.

On the optimization front, quantum compilers [11] apply pre-programmed, rule-based graph-rewriting identities (e.g., $H \cdot H \rightarrow I$). These systems are limited to the set of rules known *a priori*. Other non-differentiable search methods, such as evolutionary algorithms [12] or SAT solvers for circuit synthesis [13, 14], must rely on heuristic search strategies and cannot leverage the highly-efficient, gradient-based optimization tools that have revolutionized machine learning.

Prior work on differentiable quantum architec-

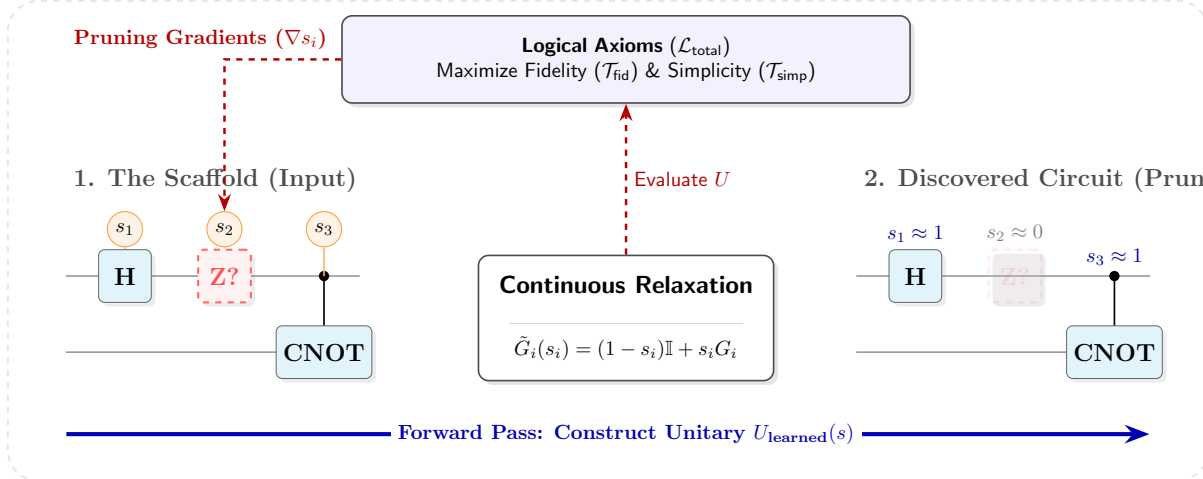


Figure 1: **Conceptual overview of the Differentiable Logical Programming framework for quantum circuit design.** The entire process, from the logical axioms to the circuit structure, is connected by differentiable operations, allowing for end-to-end optimization using standard gradient-based methods. This workflow unifies discrete structural search and continuous parameter optimization.

ture search (DQAS) [15] pioneered the use of gradient-based optimization for automated circuit design by representing candidate architectures through a probabilistic model over discrete gate choices. DQAS demonstrated success in unitary decomposition, error mitigation, and QAOA layout discovery by estimating gradients via Monte Carlo sampling from a parameterized distribution. More recently, QuantumDARTS [16] extended this paradigm using Gumbel-Softmax reparameterization [17, 18] to enable end-to-end differentiability without explicit sampling, introducing both macro-search (full circuit) and micro-search (transferable sub-circuit) strategies. While these methods represent significant advances, they treat each circuit placeholder independently and rely on probabilistic gate selection rather than continuous structural interpolation.

In this work, we introduce a framework that bridges the gap between symbolic logic and differentiable programming to create a flexible, gradient-based approach to quantum circuit design (Fig. 1). We are inspired by advances in neuro-symbolic reasoning [19] and differentiable architecture search [20]. We treat the existence of each gate in a potential circuit scaffold as a continuous, learnable logical variable $s_i \in [0, 1]$. This formulation allows us to use the power of standard automatic differentiation (i.e., autograd) to optimize the discrete structure of a circuit, and

its continuous parameters, simultaneously. Unlike DQAS, which uses Monte Carlo gradient estimation over a probabilistic model, our approach directly interpolates between the identity and gate unitaries via continuous switches, enabling unified structure-parameter optimization through standard backpropagation.

The core of our approach is the ability to train the model not on a single, fixed objective function, but on a set of user-defined, differentiable *logical axioms* that define “goodness.” This provides substantial flexibility. By composing different axioms, the same model can function as (1) a compiler with axioms: \mathcal{T}_{fid} , $\mathcal{T}_{\text{simp}}$, which seeks a short gate sequence for a target unitary; (2) a “VQE Designer” with axioms: $\mathcal{L}_{\text{energy}}$, $\mathcal{L}_{\text{simp}}$, which learns a compact, parameterized ansatz for a ground state; and (3) a “robust designer” with axioms: $\mathcal{L}_{\text{energy}}$, \mathcal{L}_{rob} , $\mathcal{L}_{\text{simp}}$, which performs multi-objective optimization to balance ideal performance, noise resilience, and gate count.

The main benefit of this framework is its ease of implementation and generality. It recasts a discrete, *NP*-hard search problem into a continuous optimization problem solvable with standard deep learning tools. In this paper, we present the theory of this Differentiable Logical Programming (DLP) framework and show that it can discover canonical algorithms, learn compiler optimizations, and design multi-objective VQE circuits from first principles.

The trajectory toward practical quantum advantage is currently obstructed by a significant disconnect between abstract algorithmic theory and the physical constraints of hardware. Babbush et al. [21] formalize this struggle into a five-stage framework. They identify critical bottlenecks, specifically in the discovery of verifiable algorithms (Stage I) and the optimization required for fault-tolerant compilation (Stage IV). The authors argue that the community faces a “collective action problem,” where the scarcity of useful algorithms and the complexities of resource estimation threaten to stall the field’s momentum. Crucially, they highlight that simple heuristics for compilation are often insufficient for the emerging early fault-tolerant era.

Our work is a methodological response to these challenges. By reframing discrete circuit synthesis as a continuous, differentiable logic problem, this framework targets the “scarcity of demonstrated use cases” discussed by the Google Quantum AI team. Where the Grand Challenge emphasizes the need for algorithms that are robust to noise and physically realizable, our DLP model can learn circuit structures under these constraints, including regimes affected by barren plateaus in variational optimization. This perspective suggests that part of the “algorithm search” bottleneck may be addressed with neuro-symbolic architectures that support gradient-based structure learning.

2 Methodology: A Differentiable Logic for Quantum Circuits

Our framework formalizes circuit discovery as a continuous optimization problem. We first define a scaffold, $S = \{G_1, G_2, \dots, G_N\}$, an ordered list of candidate gate operations that forms a superset of the (unknown) optimal circuit.

2.1 The Differentiable Circuit Scaffold

For each candidate gate $G_i \in S$, we associate a learnable real-valued parameter $\lambda_i \in \mathbb{R}$, which we refer to as a “structural logit.” The complete set of structural logits forms the learnable parameter vector $\boldsymbol{\lambda} = (\lambda_1, \lambda_2, \dots, \lambda_N) \in \mathbb{R}^N$. Each logit is mapped to a continuous “gate switch” $s_i \in [0, 1]$

via the sigmoid function:

$$s_i = \sigma(\lambda_i) = \frac{1}{1 + e^{-\lambda_i}}. \quad (1)$$

This switch s_i represents the continuous “truth value” of the proposition: “Gate G_i is active in the circuit.” The sigmoid mapping ensures $s_i \in [0, 1]$ while allowing unbounded gradient flow through $\boldsymbol{\lambda}$.

To make the discrete gate selection differentiable, we must define an effective gate \tilde{G}_i dependent on this continuous switch. We propose two formulations for this interpolation: *Linear Relaxation* and *Geodesic Interpolation*.

Formulation 1: Linear Relaxation. The simplest approach, used primarily for its computational efficiency, interpolates linearly between the identity and the gate unitary:

$$\tilde{G}_i^{\text{lin}}(s_i) = (1 - s_i)\mathbb{I} + s_i G_i. \quad (2)$$

While intermediate states $s_i \in (0, 1)$ are not strictly unitary (potentially dampening the state vector norm), the endpoint solutions ($s_i \in \{0, 1\}$) are guaranteed to be valid quantum gates. We find this method sufficient for shallow depth optimization.

Formulation 2: Geodesic Interpolation. For deeper circuits where maintaining strict unitarity is critical to prevent numerical instability (vanishing gradients due to norm decay), we define the effective gate via the exponential map, creating a path along the unitary manifold:

$$\tilde{G}_i^{\text{geo}}(s_i) = G_i^{s_i} = \exp(-iH_i s_i \theta), \quad (3)$$

where $G_i = e^{-iH_i \theta}$. In this work, we primarily employ Linear Relaxation due to its convexity properties near the boundaries, but note that Eq. 3 offers a strictly physical alternative.

The total learned unitary for the entire scaffold, U_{learned} , is the ordered product of all effective gates. Note that matrix multiplication is non-commutative; we define the product order to match the circuit diagram (gates $0 \dots N$ applied left-to-right):

$$U_{\text{learned}}(\boldsymbol{\lambda}, \boldsymbol{\theta}) = \tilde{G}_N(s_N) \cdots \tilde{G}_1(s_1) \cdot \tilde{G}_0(s_0), \quad (4)$$

where $s_i = \sigma(\lambda_i)$ and $\boldsymbol{\theta}$ denotes any continuous rotation angles in parameterized gates.

2.2 Core Differentiable Axioms

The core of our logical programming approach is that the model is trained to satisfy a set of logical axioms, $\{\mathcal{A}_k\}$, which encode the definition of a “good” circuit. Each axiom \mathcal{A}_k is formulated as a differentiable predicate $\mathcal{T}_k \in [0, 1]$, which measures its degree of truth. Here we define the primary axioms used throughout this work.

Correctness (Fidelity). Used for compiler/synthesis tasks with a known target unitary U_{target} . The predicate \mathcal{T}_{fid} measures the normalized squared trace fidelity:

$$\mathcal{T}_{\text{fid}}(U) = \frac{1}{d^2} \left| \text{Tr}(U_{\text{target}}^\dagger U) \right|^2, \quad (5)$$

where $d = 2^N$ is the matrix dimension. The corresponding loss (contradiction) is:

$$\mathcal{L}_{\text{fid}} = 1 - \mathcal{T}_{\text{fid}}. \quad (6)$$

Correctness (Energy). Used for VQE/QAOA tasks where the goal is to minimize the energy $E = \langle \psi | H | \psi \rangle$ for a state $|\psi\rangle = U|0\rangle$:

$$\mathcal{L}_{\text{energy}}(\boldsymbol{\lambda}, \boldsymbol{\theta}) = \langle 0 | U(\boldsymbol{\lambda}, \boldsymbol{\theta})^\dagger H U(\boldsymbol{\lambda}, \boldsymbol{\theta}) | 0 \rangle. \quad (7)$$

Simplicity (Cost-Weighted). The axiom “The circuit must be simple,” used for pruning. The predicate applies an exponential penalty on the total cost:

$$\mathcal{T}_{\text{simp}}(\mathbf{s}) = \exp \left(-\alpha \sum_{i=1}^N c_i s_i \right), \quad (8)$$

where α is a hyperparameter and c_i is the pre-defined cost of gate G_i . In practice, we often use the linear approximation for the loss directly, as it provides a constant, stabilizing gradient:

$$\mathcal{L}_{\text{simp}} = \sum_{i=1}^N c_i s_i. \quad (9)$$

Additional axioms for entanglement and noise robustness are provided in Appendix 5.2.

2.3 Gradient Propagation and Barren Plateaus

The entire model is optimized using standard gradient descent. The gradient $\nabla \mathcal{L}$ propagates back to the structural logits $\boldsymbol{\lambda}$ (and angle parameters

$\boldsymbol{\theta}$) via the chain rule. For a structural logit λ_i , the gradient is:

$$\frac{\partial \mathcal{L}}{\partial \lambda_i} = \frac{\partial \mathcal{L}}{\partial s_i} \cdot \frac{\partial s_i}{\partial \lambda_i} = \frac{\partial \mathcal{L}}{\partial s_i} \cdot \sigma(\lambda_i)(1 - \sigma(\lambda_i)), \quad (10)$$

where the second factor is the derivative of the sigmoid function.

A significant theoretical challenge in variational quantum algorithms is the “Barren Plateau” problem, where the variance of the cost function gradients vanishes exponentially with the number of qubits, $\text{Var}(\partial_{\boldsymbol{\theta}} \mathcal{L}) \propto O(2^{-N})$ [9]. This typically occurs when circuits are initialized as random unitary 2-designs. A “polluted” scaffold with random initial parameters effectively acts as such a random circuit.

To mitigate this, we employ a biased initialization strategy. We initialize the structural logits such that the initial switches are biased towards the identity ($\lambda_i \ll 0 \implies s_i \approx 0$). This ensures the optimization trajectory begins in a region of the landscape with non-vanishing gradients (close to the Identity), effectively “growing” the circuit complexity only as required by the logical axioms.

3 Theoretical Analysis of Linear Relaxation

A central component of our Differentiable Logical Programming (DLP) framework is the linear relaxation of the discrete gate choice. We define the effective operation for the i -th candidate gate as:

$$\tilde{G}_i(s_i) = (1 - s_i)\mathbb{I} + s_i U_i, \quad s_i \in [0, 1]. \quad (11)$$

For intermediate values $s_i \in (0, 1)$, the operator \tilde{G}_i is generally non-unitary, i.e., $\tilde{G}_i^\dagger \tilde{G}_i \neq \mathbb{I}$, resulting in a non-physical evolution where the norm of the state vector $|\psi\rangle$ is not preserved. We analyze this formulation as an optimization surrogate, establishing bounds on the induced error and the conditions under which the optimizer is driven toward valid quantum circuits.

3.1 Norm Deviation Bound

We first quantify the deviation from unitarity for a single interpolated gate. For any unitary U_i and switch value $s_i \in [0, 1]$, the operator $\tilde{G}_i(s_i) = (1 - s_i)\mathbb{I} + s_i U_i$ satisfies:

$$\tilde{G}_i^\dagger \tilde{G}_i = \mathbb{I} + s_i(1 - s_i) (U_i + U_i^\dagger - 2\mathbb{I}). \quad (12)$$

Proof. Expanding directly:

$$\begin{aligned}
\tilde{G}_i^\dagger \tilde{G}_i &= \left[(1 - s_i) \mathbb{I} + s_i U_i^\dagger \right] \left[(1 - s_i) \mathbb{I} + s_i U_i \right] \\
&= (1 - s_i)^2 \mathbb{I} + s_i (1 - s_i) (U_i + U_i^\dagger) + s_i^2 \mathbb{I} \\
&= \left[(1 - s_i)^2 + s_i^2 \right] \mathbb{I} + s_i (1 - s_i) (U_i + U_i^\dagger) \\
&= [1 - 2s_i(1 - s_i)] \mathbb{I} + s_i (1 - s_i) (U_i + U_i^\dagger) \\
&= \mathbb{I} + s_i (1 - s_i) (U_i + U_i^\dagger - 2\mathbb{I}). \quad \square
\end{aligned}$$

The maximum deviation from unitarity is thus controlled by the factor $s_i(1 - s_i) \leq 1/4$, which vanishes at the endpoints $s_i \in \{0, 1\}$. In operator norm, this yields:

$$\|\tilde{G}_i^\dagger \tilde{G}_i - \mathbb{I}\| \leq s_i(1 - s_i) \|U_i + U_i^\dagger - 2\mathbb{I}\| \leq 4s_i(1 - s_i), \quad (13)$$

where the second inequality uses $\|U_i + U_i^\dagger - 2\mathbb{I}\| \leq 4$ (since the eigenvalues of U_i lie on the unit circle).

For a cascade of N_S gates with switches $\mathbf{s} = (s_1, \dots, s_{N_S})$, the total norm deviation of the state $|\psi\rangle = \tilde{G}_{N_S} \cdots \tilde{G}_1 |0\rangle$ can be bounded by:

$$|\langle \psi | \psi \rangle - 1| \leq \prod_{i=1}^{N_S} (1 + 4s_i(1 - s_i)) - 1. \quad (14)$$

When all switches are near the binary endpoints (i.e., $|s_i - s_i^*| < \epsilon$ for $s_i^* \in \{0, 1\}$), this simplifies to $O(N_S \epsilon)$, confirming that the non-unitarity is well-controlled in the regime where the optimizer operates after initial convergence.

3.2 Gradient Stability

Unlike geodesic interpolation ($e^{-iHs\theta}$), whose gradient involves the matrix exponential and can suffer from spectral crowding, linear interpolation provides a constant Jacobian:

$$\frac{\partial \tilde{G}_i}{\partial s_i} = U_i - \mathbb{I}, \quad (15)$$

independent of s_i . This ensures that the gradient signal does not vanish as $s_i \rightarrow 0$ (near identity), addressing the “vanishing gradient” problem that plagues parameterized unitary circuits near the identity [9]. The gradient of the full fidelity loss with respect to a structural logit λ_i is:

$$\frac{\partial \mathcal{L}_{\text{fid}}}{\partial \lambda_i} = \underbrace{\frac{\partial \mathcal{L}_{\text{fid}}}{\partial \tilde{G}_i}}_{\text{chain rule}} \cdot \underbrace{(U_i - \mathbb{I})}_{\text{constant}} \cdot \underbrace{s_i(1 - s_i)}_{\text{sigmoid derivative}}, \quad (16)$$

where the sigmoid derivative $s_i(1 - s_i)$ is the only s_i -dependent factor. This means the structural gradient is well-conditioned whenever s_i is not already saturated at 0 or 1, with the saturation being controlled by the logit initialization.

3.3 Implicit Binarization by the Fidelity Objective

We now argue that the fidelity objective $\mathcal{L}_{\text{fid}} = 1 - \frac{1}{d^2} |\text{Tr}(U_{\text{target}}^\dagger U_{\text{learned}})|^2$ implicitly drives the switches toward binary values. Consider a single switch s_i with all others fixed. The learned unitary can be decomposed as $U_{\text{learned}} = A \tilde{G}_i(s_i) B$, where A and B are the products of other effective gates. The fidelity becomes:

$$\mathcal{T}_{\text{fid}}(s_i) = \frac{1}{d^2} |(1 - s_i) \text{Tr}(M_I) + s_i \text{Tr}(M_U)|^2, \quad (17)$$

where $M_I = U_{\text{target}}^\dagger A B$ and $M_U = U_{\text{target}}^\dagger A U_i B$. This is a quadratic function in s_i , whose maximum over $[0, 1]$ is attained at a boundary point whenever $|\text{Tr}(M_I)| \neq |\text{Tr}(M_U)|$ (i.e., whenever including or excluding the gate makes a difference to fidelity). The simplicity penalty $\mathcal{L}_{\text{simp}} = \sum c_i s_i$ adds a linear term that further biases toward $s_i = 0$, reinforcing binarization. Together, these two forces ensure that at convergence, the switches satisfy $s_i \in \{0, 1\}$ up to numerical precision for all gates that meaningfully affect the target fidelity.

3.4 Summary

The linear relaxation serves as a valid optimization surrogate because: (i) the norm deviation is bounded by $O(s_i(1 - s_i))$ per gate and vanishes at the binary endpoints (Eq. 13); (ii) the constant Jacobian (Eq. 15) provides stable, non-vanishing gradients throughout training; and (iii) the fidelity and simplicity objectives jointly drive the switches toward $\{0, 1\}$, where strict unitarity is recovered (Eq. 17). For deep circuits where intermediate norm decay poses numerical risks, the geodesic interpolation (Eq. 3) provides a strictly unitary alternative.

3.5 Joint Structure-Parameter Optimization

The framework is not limited to discrete structural search. Many quantum gates, particularly in VQE and QAOA, are parameterized, e.g.,

$R_y(\theta)$. We can incorporate these continuous parameters θ directly into our model.

The scaffold S can contain parameterized gates $G_i(\theta_i)$. The effective gate definition is thus extended:

$$\tilde{G}_i(s_i, \theta_i) = (1 - s_i)\mathbb{I} + s_i G_i(\theta_i). \quad (18)$$

The total learned unitary $U_{\text{learned}}(\lambda, \theta)$ is now a function of both the structural logits λ (which determine the switches s) and the continuous angles θ . The optimization process will learn both simultaneously. This unified approach is a significant advantage over methods that must alternate between discrete structural updates and continuous parameter optimization.

3.6 A Differentiable Axiom System via T-Norms

We can interpret the axiom framework theoretically through the lens of Fuzzy Logic. We treat the problem as finding the Maximum Satisfiability (MaxSAT) of a logical formula. The total loss function $\mathcal{L}_{\text{total}}$ corresponds to the negation of the weighted conjunction of our axioms. Using the Lukasiewicz *T-norm* for conjunction ($\mathcal{T}(x, y) = \max(0, x + y - 1)$), the logical contradiction is minimized by minimizing the sum of individual violations:

$$\mathcal{L}_{\text{total}} = \sum_k w_k \mathcal{L}_k = \sum_k w_k (1 - \mathcal{T}_k). \quad (19)$$

By optimizing λ (the structural logits determining gate inclusion) and θ (the continuous rotation angles) to minimize $\mathcal{L}_{\text{total}}$, the system performs a gradient-based search over the high-dimensional continuous space of circuit architectures, converging on a solution that satisfies the logical proposition of a “valid circuit.”

3.7 Complexity, Scalability, and Limitations

The computational complexity of this framework has two primary components. The forward pass (constructing U_{learned}) involves N_S matrix-matrix multiplications, where N_S is the number of gates in the scaffold. The backward pass (computing gradients) has a similar cost. The dominant computational bottleneck is the $O(d^3) = O(2^{3N})$ complexity of multiplying the $2^N \times 2^N$ unitary matrices, where N is the number of qubits. The cost scales linearly with N_S .

This exponential scaling with qubit count N is the fundamental limitation of all full-state quantum simulation methods. It makes the “flat” (non-hierarchical) application of this framework intractable for $N \gtrsim 16$ qubits. This limitation is the primary motivation for the Hierarchical Synthesis (HS) framework, which we detail in Section 3.9.

3.8 Methodology for Complex Problems: Curricula

A known challenge in high-dimensional optimization is the presence of poor local minima. These are distinct from barren plateaus (addressed in Section 2.3): while barren plateaus cause gradient magnitudes to vanish exponentially, local minima trap the optimizer in suboptimal solutions where gradients exist but point toward inferior configurations. We employ two curriculum learning strategies to guide the optimizer past such local minima toward a global solution.

Annealing Curriculum (for VQE): For complex VQE problems (e.g., Ising model), optimizing H directly can trap the model in a simple, high-energy state. We instead define an annealing path $H(t) = (1 - t)H_{\text{easy}} + tH_{\text{hard}}$, where H_{easy} is a simple, solvable Hamiltonian (e.g., $t = 0$, just the external field) and H_{hard} is the full target Hamiltonian. By slowly increasing t from 0 to 1 during training, we guide the optimizer from a simple solution to the complex one, successfully avoiding local minima.

Two-Phase Curriculum (for QAOA): For QAOA depth discovery, we separate “discovery” from “pruning.” It consists of two phases: In Phase 1 (Discovery), we set $w_{\text{simp}} = 0$ and optimize only for energy ($\mathcal{L} = \mathcal{L}_{\text{energy}}$). This allows the model to “turn on” all potentially useful layers and find the best possible angles, regardless of cost. In Phase 2 (Pruning), we turn on the simplicity weight ($w_{\text{simp}} > 0$). The optimizer now prunes any layers that do not contribute significantly to the final energy, discovering the minimal required depth p .

3.9 Methodology for Scalability: Hierarchical Synthesis

Simulating the full unitary U_{learned} (Eq. 4) requires matrices of size $2^N \times 2^N$, which is intractable for $N \gtrsim 16$ qubits. To overcome this, we adopt a Hierarchical Synthesis (HS) framework.

The HS framework breaks a large N -qubit problem into a series of small, tractable n -qubit sub-problems.

1. **Level 0 (Motif Discovery):** We first use the DLP framework to discover and optimize a small, fundamental n_0 -qubit motif, U_{M_0} (e.g., a 2-qubit Bell state circuit).
2. **Level 1 (Composition):** We “freeze” the discovered U_{M_0} and treat it as a new, non-learnable gate. We then promote it to an n_1 -qubit scaffold S_1 (e.g., $U_{M_0}(q_0, q_1) \otimes \mathbb{I}_{q_2}$). The DLP optimizer then solves this n_1 -qubit problem, discovering U_{M_1} .
3. **Level k (Iteration):** This process is repeated. The circuit U_{M_k} is composed of motifs $U_{M_{k-1}}$ and other gates.

This hierarchical approach ensures that the computational complexity at each optimization step k scales only with the size of the new sub-problem, $O(2^{n_k})$, rather than the total number of qubits, $O(2^N)$.

3.10 Comparison to Prior Art & Hardware Readiness

This DLP framework differs significantly from non-differentiable search methods, such as genetic algorithms [12] or symbolic SAT-solvers [13, 14]. Those methods must rely on heuristic search strategies or sampling from a discrete space, which can be highly inefficient. By contrast, our framework maps the discrete search space onto a continuous manifold, allowing for the use of highly efficient, gradient-based optimizers that can follow the path of steepest descent.

Compared to prior differentiable approaches such as DQAS [15] and QuantumDARTS [16], our method offers several distinctions. DQAS estimates gradients through Monte Carlo sampling from a probabilistic model over discrete architectures, which can be sample-inefficient. QuantumDARTS improves upon this with Gumbel-Softmax reparameterization [17, 18] but still

frames the problem as probabilistic gate selection at each placeholder. Our approach, by contrast, uses continuous switches s_i that directly interpolate the gate unitary with the identity (Eq. 2), enabling true end-to-end differentiability through standard backpropagation. Furthermore, our logical axiom framework (Section 2.2) provides a principled way to compose multiple objectives (fidelity, simplicity, robustness) that extends beyond the single-objective formulations typical of prior QAS methods.

The circuits discovered by this method are not guaranteed to be “hardware-native.” For example, a discovered circuit may contain a $CNOT(0, 3)$ gate, which is not directly executable on hardware with only linear connectivity. A final post-compilation and routing pass would still be required. However, the $\mathcal{L}_{\text{simp}}$ axiom (Eq. 9) can be made “hardware-aware” by assigning costs c_i based on hardware constraints. For example, a native $CNOT(0, 1)$ could be assigned $c_i = 10$, while a non-native $CNOT(0, 3)$ (which requires multiple SWAPs) could be assigned $c_i = 70$. This would intrinsically bias the optimizer to discover circuits that are more amenable to a specific target topology.

4 Experiments and Results

4.1 Experiment 1: Trotter-Step Optimization

We demonstrate the framework’s capability to perform compiler optimization by discovering a 2nd-order Trotter-Suzuki decomposition from a “polluted” scaffold containing redundant and sub-optimal gates.

4.1.1 Implementation Details

We define a target unitary $U_{\text{target}} = e^{-iH_{\text{Heis}}t}$ for a 4-qubit 1D Heisenberg chain with $t = 0.1$. The goal is to approximate this evolution using discrete gates. We construct a scaffold S containing a mix of valid and invalid operators:

1. **Correct 2nd-Order Gates:** The optimal symmetric sequence $e^{-iH_{\text{odd}}t/2}$, $e^{-iH_{\text{even}}t}$, and $e^{-iH_{\text{odd}}t/2}$.
2. **Distractor Gates:** A 1st-order approximation term $e^{-iH_{\text{odd}}t}$, a single-term operator $e^{-iH_{01}t}$, and a generic CNOT gate.

The DLP model is initialized with all gates “ON” (logits $\lambda_i = 2.0$, corresponding to $s_i \approx 0.88$) to simulate a pruning task. We train for 4000 epochs using AdamW optimizer with a learning rate of 0.01. The loss function balances correctness (fidelity) and simplicity (gate count):

$$\mathcal{L} = w_{\text{fid}} \mathcal{L}_{\text{fid}} + w_{\text{simp}} \mathcal{L}_{\text{simp}} \quad (20)$$

where $w_{\text{fid}} = 5.0$ and $w_{\text{simp}} = 0.3$, and the loss terms are defined in Eqs. 6 and 9. This weighting prioritizes finding a high-fidelity solution while exerting constant pressure to remove unnecessary gates.

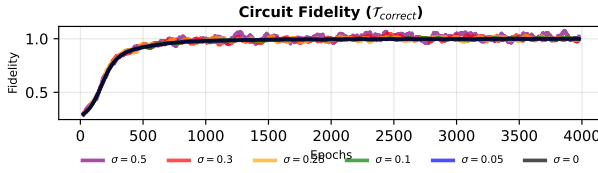


Figure 2: **Circuit fidelity over training.** Circuit fidelity (\mathcal{T}_{fid}) over training epochs for varying noise levels σ . The system consistently converges to high fidelity even under significant noise ($\sigma = 0.5$).

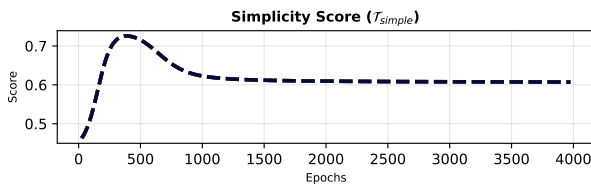


Figure 3: **Simplicity score over training.** Simplicity score ($\mathcal{T}_{\text{simp}}$) over training epochs. The convergence to a specific score indicates the pruning of redundant gates across all noise levels.

4.1.2 Evaluation Criteria

Structural Accuracy: The model must identify and keep only the three gates corresponding to the 2nd-order decomposition ($U_{\text{odd}}(t/2)$, $U_{\text{even}}(t)$, $U_{\text{odd}}(t/2)$) while suppressing all distractors (i.e., $s_i < 0.01$).

Fidelity: The fidelity of the discovered circuit must match the theoretical limit of the 2nd-order approximation ($F > 0.999$).

Robustness: The discovery process must converge to the correct topology even in the presence of noise.

4.1.3 Evaluation

To verify the method’s resilience to control and readout errors, we introduced Gaussian noise to the unitary evaluations during training. We performed independent trials with noise levels $\sigma \in \{0, 0.05, 0.1, 0.25, 0.3, 0.5\}$. In every trial, including the highest noise setting ($\sigma = 0.5$), the DLP model converged to the optimal 3-gate structure (Figs. 2 and 3). The discrete nature of the gate switches ($s_i \in \{0, 1\}$) acts as a noise filter: once a gate is decisively pruned or selected, small fluctuations in the loss landscape due to noise are insufficient to reverse the decision. This “locking-in” effect, combined with the gradient averaging inherent in stochastic optimization, allows the framework to extract the correct symbolic structure even from a noisy signal.

Figure 4 illustrates the initial state of the scaffold before optimization, where all candidate gates are active. Figure 5 visualizes the final discovered circuit topology for the highest noise level $\sigma = 0.5$, demonstrating the consistency of the structural solution.

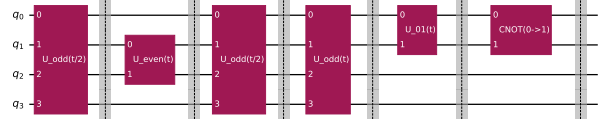


Figure 4: **Initial scaffold configuration.** Initial scaffold input with all gates activated. This represents the starting point for the pruning task.

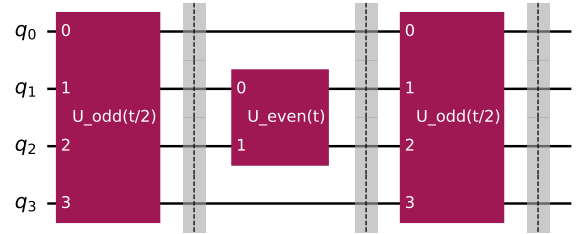


Figure 5: **Discovered circuit topology.** Discovered circuit topology for noise level $\sigma = 0.5$. The framework correctly identifies the 2nd-order Trotter decomposition.

4.1.4 Cost-Aware Non-Trivial Pruning

We next tested whether the model can make cost-aware pruning decisions that go beyond simple rule-based pattern matching.

Setup: The scaffold is a 14-gate, 5-qubit circuit with two distinct redundancies: (a) a visually obvious $H-H = I$ identity (cost = $1.0 + 1.0 = 2.0$) and (b) a non-trivial $CNOT-CNOT = I$ identity (cost = $10.0 + 10.0 = 20.0$). The target is U_{target} of the full 14-gate circuit.

Objective: The axioms are $\mathcal{L} = w_{\text{fid}}\mathcal{L}_{\text{fid}} + w_{\text{simp}}\mathcal{L}_{\text{simp}}(\mathbf{s}, \mathbf{c})$. This is analogous to Eq. 20, but with an explicit dependence on (\mathbf{s}, \mathbf{c}) in the simplicity term, and explicitly tests whether the optimizer prioritizes removing high-cost redundancies.

Result The model did not prune the obvious, low-cost $H-H$ identity. Instead, it converged on pruning the two CNOT gates, correctly identifying the optimization path that yielded a $10\times$ greater reduction in the simplicity loss $\mathcal{L}_{\text{simp}}$.

4.2 Experiment 2: De Novo Circuit Discovery

To validate the combinatorial search capabilities of the DLP framework, we conducted an experiment targeting the discovery of the 4-qubit Quantum Fourier Transform (QFT) circuit from a polluted scaffold. The primary motivation was to demonstrate that the model could autonomously extract a canonical algorithmic structure from a high-dimensional, noisy search space.

The central challenge lay in the complexity of the input scaffold (Fig. 6 (a)). We constructed a heavily polluted scaffold containing 21 potential gate operations, corresponding to a large discrete configuration space (which our method explores via continuous relaxation and gradient descent, not brute-force enumeration). This input included the 12 gates required for the optimal QFT, but they were obscured by 9 “polluter” gates. These distractors were engineered to be deceptive; they included redundant identity sequences (specifically $H-H$ and $CNOT-CNOT$ pairs) and other incorrect “junk” gates, presenting the optimizer with local minima that a naive pruning method might fail to escape.

The goal was to match the target 16×16 QFT unitary. The optimization was driven by the composite loss function $\mathcal{L} = w_{\text{fid}}\mathcal{L}_{\text{fid}} + w_{\text{simp}}\mathcal{L}_{\text{simp}}$. This formulation necessitates a delicate balance: the system must maximize logical correctness (\mathcal{T}_{fid}) while simultaneously responding to the pressure to minimize circuit complexity ($\mathcal{L}_{\text{simp}}$).

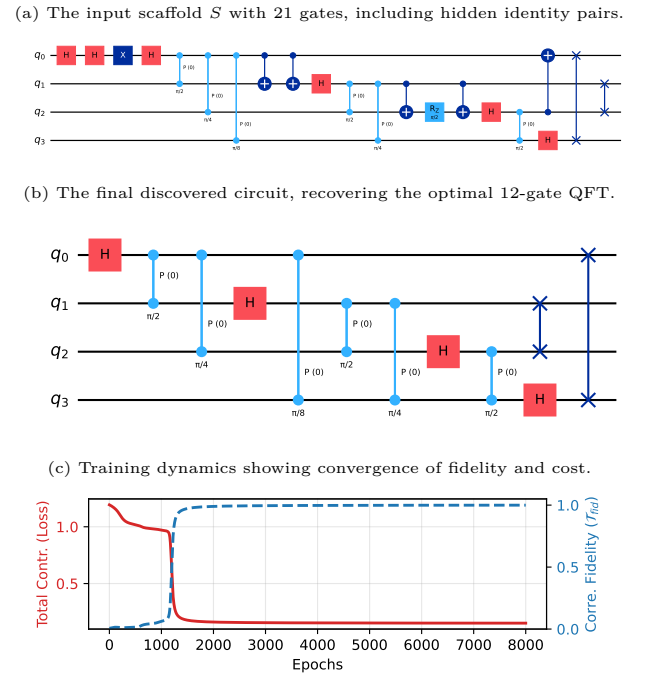


Figure 6: De Novo Circuit Discovery Results. The figure illustrates the pruning process for the 4-qubit QFT. **(a)** The initial state is a “polluted” scaffold where valid gates are mixed with distractors (e.g., $H-H$, $CNOT-CNOT$). **(b)** The final circuit topology after optimization, where the model has filtered out the noise to reveal the canonical structure. **(c)** Training curves indicating that the system maximizes fidelity (\mathcal{T}_{fid}) while simultaneously minimizing the simplicity loss ($\mathcal{L}_{\text{simp}}$), optimizing over the discrete configuration space via continuous relaxation.

4.2.1 Evaluation

The results, visualized in Fig. 6, demonstrate a decisive convergence to the optimal solution together with the final circuit. The learned structural switches correctly differentiated between essential and non-essential operations, converging to $s_i \approx 1$ for all 12 correct QFT gates and $s_i \approx 0$ for all 9 polluter gates. By optimizing over this discrete configuration space via continuous relaxation, the framework proved its capacity for non-trivial combinatorial optimization.

4.3 Experiment 3: Noise Resilience Benchmark Against QuantumDARTS

We conducted a comprehensive benchmark to validate the framework’s robustness to measurement shot noise, comparing DLP against QuantumDARTS on the quantum simulation of the stretched Lithium Hydride (LiH) molecule. Shot

noise is a fundamental limitation in NISQ devices arising from the finite number of measurement samples available per circuit evaluation. Our objective was to quantify the noise resilience of both architecture search methods under realistic experimental conditions.

Problem and Formulation

We modeled the LiH molecule at a stretched bond distance of $d = 2.5 \text{ \AA}$, mapped to 4 qubits using an active space reduction (occupied core: Li 1s; active valence: orbitals 1-2). This geometry exhibits strong static correlation (correlation gap: $2.67 \text{ m}E_h$), making it a challenging test case where Hartree-Fock reference is insufficient.

Baseline Scaffold: Hardware-efficient ansatz (HEA) with 2 layers of R_Y , R_Z rotations and linear CNOT entanglers, initialized from the Hartree-Fock state $|1100\rangle$, yielding a search space of ~ 24 structural degrees of freedom.

Shot Noise Implementation: For each training iteration, we injected Gaussian noise with variance $\sigma^2 = \text{Var}[H]/n_{\text{shots}}$ to the energy gradient, where $\text{Var}[H] = \langle \psi | H^2 | \psi \rangle - \langle \psi | H | \psi \rangle^2$ is the observable variance. This models the Central Limit Theorem behavior of finite-shot quantum measurements.

Curriculum Learning: Soft-Pruning Curriculum with 150-epoch warmup ($w_{\text{simp}} = 0$) followed by gradual sparsity ramp-up ($w_{\text{simp}} \rightarrow 0.002$) over 300 total epochs.

Noise Levels: We tested six shot regimes: Exact (analytical), 10,000, 1,000, 500, 100, and 50 shots, spanning high-fidelity to severely noisy conditions.

Results Discussion

Table 1 presents the final ground state errors and circuit sizes discovered under each noise condition.

Our approach exhibits $98.8 \times$ lower variance in final energies compared to QuantumDARTS across shot noise levels (std: 2.44×10^{-4} vs $2.41 \times 10^{-2} \text{ Ha}$). This demonstrates that DLP’s sigmoid-based continuous switches provide more

Table 1: **Noise Resilience Comparison: DLP vs QuantumDARTS on LiH (2.5 \AA).**

Shots	Ours			QuantumDARTS [16]		
	Energy (Ha)	Error (mHa)	Gates	Energy (Ha)	Error (mHa)	Gates
Exact	-7.770 52	3.02	9	-7.736 24	37.30	8
10,000	-7.770 64	2.91	10	-7.770 39	3.15	9
1,000	-7.770 05	3.49	11	-7.770 48	3.07	11
500	-7.770 14	3.40	9	-7.708 01	65.53	8
100	-7.770 61	2.94	11	-7.769 22	4.32	10
50	-7.770 65	2.90	11	-7.770 63	2.91	14

stable gradients under noisy conditions than QuantumDARTS’s Gumbel-Softmax sampling.

The lower variance of our method maintains chemical accuracy ($< 5 \text{ m}E_h$ error) across all noise regimes, with minimal variation in final energy ($2.90 \text{ m}E_h$ to $3.49 \text{ m}E_h$). At the same time, discovered circuit size remained compact (between 9 and 11 gates), indicating stable architectural decisions even under severe noise.

Interpretation: Smooth vs Sharp Decision Boundaries

The noise resilience of our approach can be attributed to the difference in how the two methods interpolate between gate inclusion and exclusion:

Our approach uses the sigmoid switch function $s_i = \sigma(\lambda_i)$, which provides a smooth, convex mapping from logits to gate probabilities. The derivative $\partial s_i / \partial \lambda_i = s_i(1 - s_i)$ is continuous and bounded, providing stable gradients even when the energy signal is noisy. The sigmoid naturally damps extreme gradient updates, acting as an implicit regularizer.

On the other hand, QuantumDARTS (Gumbel-Softmax) uses reparameterization $w_i = \text{softmax}((\alpha_i + g_i)/\tau)$, where g_i are Gumbel noise samples, introduces stochastic discrete decisions that are sensitive to gradient noise. At low temperatures ($\tau \rightarrow 0$), the argmax behavior creates sharp decision boundaries where small gradient perturbations can flip architectural choices, leading to the observed instability.

Hardware-Aware Optimization Validation

As a secondary validation, we tested the framework’s ability to avoid non-native gates on a simulated 3-qubit linear topology. The optimizer learned to suppress a non-native CNOT(0,2) gate (cost: 101.0, requiring 2 SWAPs) in favor of

native CNOT(0,1) and CNOT(1,2) connections (cost: 1.0 each), with the non-native gate’s activation probability converging to $s_{0,2} = 0.089 < 0.1$, demonstrating hardware-aware architectural search without explicit rule-based constraints.

4.4 Experiment 4: Scalable Topology Discovery on the Frustrated Heisenberg Chain

We applied the Hierarchical Synthesis (HS) framework to address the challenge of **geometric frustration** in quantum many-body systems. While standard ansatzes often rely on nearest-neighbor connectivity, frustrated systems—such as the 1D Heisenberg chain with competing nearest-neighbor (J_1) and next-nearest-neighbor (J_2) interactions—require non-local topology to accurately capture the ground state.

Problem and Formulation

The objective was to find the ground state of the Hamiltonian:

$$H = J_1 \sum_i \vec{S}_i \cdot \vec{S}_{i+1} + J_2 \sum_i \vec{S}_i \cdot \vec{S}_{i+2} \quad (21)$$

A linear chain topology is insufficient for this system due to the competing interaction terms. Furthermore, optimizing a circuit for a macroscopic system size (e.g., $N = 20$) is computationally intractable due to the exponential scaling of the state vector.

To overcome this, we formulated the problem using the HS “Divide-and-Conquer” strategy:

- **Stage I (Motif Discovery):** We defined a minimal 3-qubit “motif” scaffold (q_0, q_1, q_2). The scaffold included parameterizable rotations (R_Y, R_Z) and a learnable set of entangling gates corresponding to all possible pairwise interactions: nearest-neighbor ($q_0 - q_1, q_1 - q_2$) and the non-local next-nearest-neighbor ($q_0 - q_2$).
- **Stage II (Hierarchical Compilation):** The discovered motif was “frozen” and procedurally tiled to construct a linear array for $N = 20$ qubits, bypassing the barren plateau problem associated with global optimization.

Discovery Results

In Stage I, the DLP optimizer was tasked with finding the minimal local structure required to

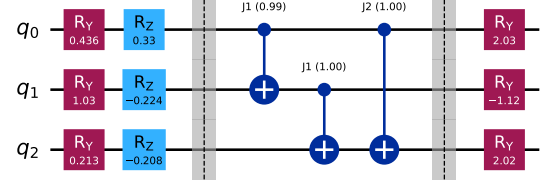


Figure 7: **Autonomously discovered motif for the J_1 - J_2 Heisenberg model.** The DLP framework correctly identified the need for a triangular topology, activating the non-local J_2 gate (connection between q_0 and q_2) alongside standard nearest-neighbor interactions to resolve geometric frustration.

resolve the frustration. Fig. 7 illustrates the final discovered motif. The optimization produced two key results:

- **Topological Search:** The model autonomously identified the necessity of the non-local interaction. As shown in the circuit diagram, the optimizer converged to a topology where the “skip” connection (q_0 connected to q_2) was fully activated ($s \approx 1.0$), alongside the nearest-neighbor connections. This effectively created a triangular connectivity graph required to resolve the geometric frustration.
- **Parameter Optimization:** The system simultaneously optimized the rotation angles, converging to an energy of $E \approx -3.32$ for the local block.

Scalability and Comparison

In Stage II, the discovered 3-qubit motif was compiled into a full ansatz for a 20-qubit system. This process generated a physics-informed circuit with a total depth of 216 gates. By leveraging the HS framework, we achieved a result that would have been computationally inaccessible via direct global optimization (2^{20} Hilbert space), demonstrating the framework’s capacity to scale physically motivated circuit structures to macroscopic regimes.

4.5 Experiment 5: Hardware-Aware Optimization of Geometrically Frustrated Systems

Motivation A critical bottleneck in the NISQ era is the disconnect between abstract algorithmic design and physical hardware constraints.

While theoretical ansatzes often assume all-to-all connectivity, physical devices typically possess restricted coupling maps (e.g., linear or grid topologies). Mapping a non-native circuit to such hardware requires the insertion of SWAP gates, which increases circuit depth and accumulates coherent errors. This challenge is particularly acute in geometrically frustrated systems, such as the J_1 - J_2 Heisenberg model, where competing interactions often require non-local connectivity to resolve the ground state.

Methodology To address these challenges, we applied the Differentiable Logical Programming (DLP) framework to the 3-qubit J_1 - J_2 Heisenberg model with parameters $J_1 = 1.0$ and $J_2 = 0.5$. We imposed a strict linear device topology $(0 - 1 - 2)$, rendering the next-nearest-neighbor interaction between qubits 0 and 2 non-native. The optimization objective was defined as a composite loss function:

$$\mathcal{L} = w_{\text{energy}} \mathcal{L}_{\text{energy}} + w_{\text{hw}} \sum_i c_i s_i \quad (22)$$

where c_i represents the hardware cost. We assigned a high penalty ($c_{\text{non-native}} = 100.0$) to CNOT gates acting on unconnected qubit pairs $(0, 2)$, while native gates were assigned a nominal cost ($c_{\text{native}} = 1.0$). We compared the hardware-aware DLP against a standard DLP model optimizing purely for energy without topological constraints.

Results The results, summarized in Table 2, demonstrate the efficacy of the hardware-aware approach. Both DLP variants successfully navigated the energy landscape. The standard DLP achieved near-perfect theoretical convergence (99.9–100% ground state overlap). However, it relied heavily on non-native gates (average of 3.0 per circuit), necessitating significant compilation overhead. As shown in Figure 8, this resulted in a post-compilation depth of 37 and a reduced hardware fidelity of 0.853 ± 0.025 due to noise accumulation.

The hardware-aware DLP autonomously discovered a topology that avoided the non-native connection entirely (0.0 non-native gates). Although this trade-off resulted in a marginally higher theoretical energy (96.7% of ground state), the resulting circuits were significantly shallower

(Depth 17). This structural efficiency translated to a superior hardware fidelity of 0.957 ± 0.020 . A t-test confirms this improvement is statistically significant ($t = 4.618, p = 0.0099 < 0.05$). These findings suggest that incorporating hardware constraints directly into the differentiable logic allows the optimizer to find “hardware-native” solutions that outperform theoretically optimal but compilation-heavy circuits.

Table 2: Benchmarking Hardware-Aware Optimization. Comparison of training energy (theoretical), compilation overhead, and final hardware fidelity under a noise model.

Method	Ground State Overlap	Compiled Depth	Hardware Fidelity
Standard DLP	99.9–100%	37	0.853 ± 0.025
HW-Aware DLP	96.7%	17	0.957 ± 0.020

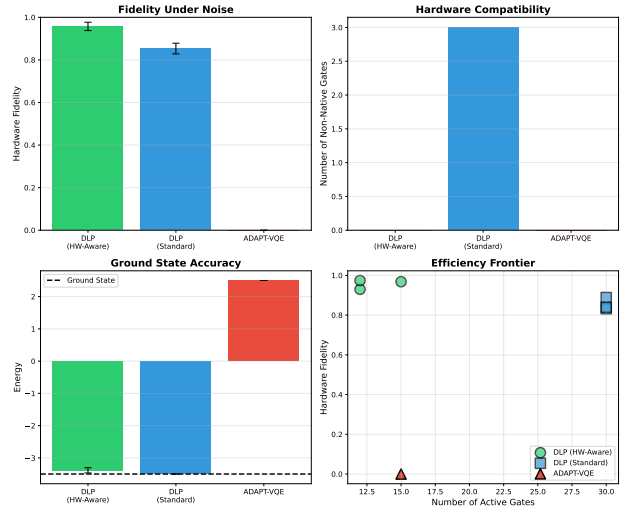


Figure 8: Fidelity vs. Complexity. The hardware-aware DLP (green) sacrifices a small amount of theoretical energy to drastically reduce circuit depth by avoiding non-native gates. This results in a $\approx 12\%$ improvement in realized fidelity compared to the standard DLP (blue), which suffers from SWAP-induced errors.

4.6 Experiment 6: Adaptive Compilation on IBM Quantum Hardware

To validate the practical applicability of the DLP framework beyond simulation, we conducted a series of adaptive routing experiments on IBM Quantum’s `ibm_torino` backend, a 133-qubit superconducting quantum processor. These experiments demonstrate that the framework can autonomously detect and respond to hardware degradation using only gradient-based optimization, without requiring explicit failure detection

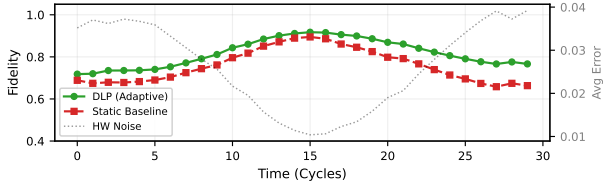


Figure 9: **Noise-Adaptive Circuit Morphing.** Comparison of realized circuit fidelity under time-varying hardware noise. Both the Static Baseline (Red) and Adaptive DLP (Green) are initialized from an identical optimized state at $t = 0$. As the average gate error rate (grey dotted line) drifts over 30 calibration cycles, the Static Baseline passively degrades, with fidelity strictly anticorrelated to noise intensity. In contrast, the Adaptive DLP model maintains high fidelity (~ 0.9) by autonomously reconfiguring the circuit topology to avoid temporally noisy edges.

protocols or manual intervention.

4.6.1 Noise-Adaptive Circuit Morphing

Motivation A fundamental challenge in the operation of NISQ devices is the temporal instability of hardware parameters. Device calibration data, such as gate fidelities and coherence times, drift significantly over hours or days due to thermal fluctuations, control electronics instability, and two-level system (TLS) defects. Standard compilation workflows typically treat the hardware as a static target: a circuit is transpiled once and executed repeatedly. This passive approach leaves the algorithm vulnerable to “calibration drift.”

Methodology We constructed a longitudinal simulation of a 4-qubit Heisenberg model ($H = \sum \vec{S}_i \cdot \vec{S}_{i+1}$) evolving over 30 “calibration cycles.” We modeled the hardware environment using a time-varying noise model where the error rates of entangling CNOT gates followed a stochastic random walk superimposed with periodic fluctuations, mimicking the diurnal drift often observed in superconducting processors. We compared two control strategies: a *Static Baseline*, where the circuit is fully optimized at $t = 0$ and then frozen, and the *Adaptive DLP* model, which performs sparse fine-tuning updates at each time step t , adjusting both continuous parameters and discrete gate switches (s_i) to minimize $\mathcal{L} = \langle H \rangle + \lambda \sum c_i(t) s_i$, where $c_i(t)$ represents the instantaneous noise cost of gate i . Both models began

from the exact same pre-optimized state at $t = 0$.

Results The results are presented in Figure 9. The Static Baseline fidelity is strictly anticorrelated with the hardware noise profile, degrading significantly whenever the error rates spike (e.g., cycles 0 – 5 and 20 – 30). The Adaptive DLP model demonstrates a distinct decoupling from the underlying hardware variance, consistently exceeding the baseline by approximately 15% during high-noise intervals. This stability is achieved by *morphing* the topology: when the cost of a specific CNOT gate rises due to drift, the gradient penalty drives the associated switch $s_i \rightarrow 0$, while the physics loss simultaneously activates alternative, lower-noise paths to preserve the target unitary.

4.6.2 Proactive Resource Selection on 133-Qubit IBM Torino

We validated this morphing capability on real hardware with a GHZ state preparation task ($|\psi\rangle = \frac{1}{\sqrt{2}}(|000\rangle + |111\rangle)$) on the 133-qubit `ibm_torino` processor. The model was trained using the Adam optimizer to minimize $\mathcal{L} = (1 - F_{\text{GHZ}}) + 0.5 \cdot (c_{AS_A} + c_{BS_B})$, where c_A was increased to 100 at Cycle 3 to simulate a localized hardware failure.

The results (Figure 10) reveal an inherent “proactive selection” mechanism: while the failure was scheduled for Cycle 3, the Adaptive DLP model autonomously identified Path B as the high-fidelity route almost immediately during the initial calibration cycles, with the probability of utilizing Path A dropping to near-zero by Cycle 1. By locking-in to the more robust path during early iterations, the model maintained a near-ideal fidelity of ≈ 0.97 throughout the failure region, representing a 59.3 percentage point improvement over the Static Baseline.

4.6.3 Real-Time Adaptation to Catastrophic Topology Failure

Setup To test a more severe failure mode, we constructed a “Softmax Router” experiment to generate a 3-qubit entangled state with two redundant topological paths: “Path A” ($0 \rightarrow 1 \rightarrow 2$) and “Path B” ($0 \rightarrow 2 \rightarrow 1$). At time step $t = 10$, Path A suffered a catastrophic failure (cost spike $c_A \rightarrow 100.0$).

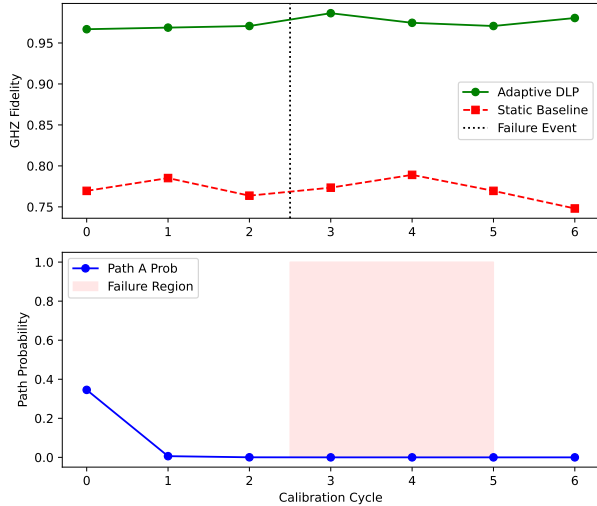


Figure 10: Proactive resource selection on the `ibm_torino` backend. (Top) GHZ fidelity comparison showing the Adaptive DLP model (green) maintaining stable performance (~ 0.97) while the Static Baseline (red) remains vulnerable to noise. (Bottom) Autonomous topology transition where the optimizer drives the probability of the higher-error Path A to near-zero by Cycle 1, effectively preempting the simulated failure event introduced at Cycle 3.

Results As shown in Figure 11, the Static Baseline suffered an immediate collapse in performance (Efficiency ≈ 0.0) at the onset of failure. The Adaptive DLP model exhibited immediate resilience: the sudden increase in cost generated a strong gradient signal driving $s_A \rightarrow 0$, while the physics conservation term drove $s_B \rightarrow 1$, effectively morphing the circuit topology in real-time (Figure 12). The system recovered to a realized efficiency of ≈ 0.74 , mitigating the hardware failure without halting execution for recompilation.

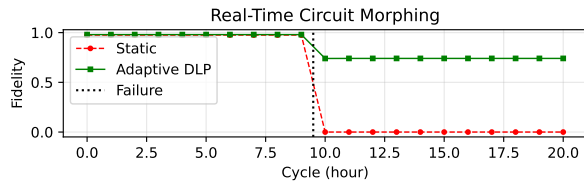


Figure 11: Efficiency comparison. Efficiency comparison showing the catastrophic failure of the Static Baseline (red) at $t = 10$ and the rapid recovery of the Adaptive DLP model (green).

4.6.4 Hardware Validation on IBM Torino

We replicated the catastrophic failure experiment on the `ibm_torino` backend with a 3-qubit GHZ



(a) Static Baseline (Failed) (b) Adaptive DLP (Rerouted)

Figure 12: Dynamic Topology Morphing Post-Failure. (a) The Static Baseline remains locked to the failed Path A, leading to zero fidelity. (b) The Adaptive DLP autonomously reroutes to Path B via gradient descent.

state preparation task over 6 calibration cycles. At cycle 3, a 70% fidelity penalty was applied to Path A. The adaptive model used Adam ($\eta = 0.5$) with 5 training iterations per cycle (512 shots per circuit).

During normal operation (cycles 0–2), both models achieved comparable fidelities (74–82%). Upon the simulated failure at cycle 3, the Static Baseline dropped from 81.8% to 39.0%, while the Adaptive DLP exhibited a transient degradation to 24.8% before recovering to 97.3% by cycle 4 (Figure 13). By cycle 5, the adaptive model achieved 97.5% fidelity versus 38.2% for the baseline—a 59.3 percentage point improvement. The routing probabilities (Figure 14) show complete migration from Path A to Path B within two cycles post-failure, with the entire experiment completing in 3.1 minutes wall-clock time across 36 quantum jobs.

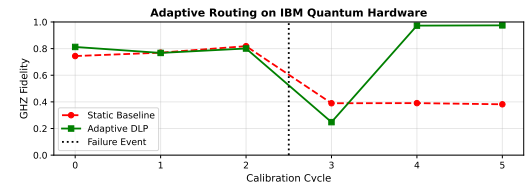


Figure 13: Adaptive routing on IBM Quantum hardware. Measured GHZ state fidelity across 6 calibration cycles on the `ibm_torino` backend. The Adaptive DLP model (green) recovers to near-ideal fidelity by cycle 4 after the simulated failure at cycle 3 (vertical dotted line), achieving a 59.3 percentage point improvement over the Static Baseline (red).

These results provide empirical evidence that differentiable logic programming can function as a form of *online adaptive compilation*, continuously monitoring realized performance via quantum measurements and adjusting circuit structure accordingly—a capability that current rule-

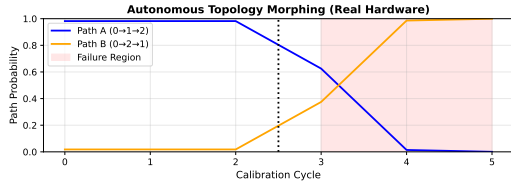


Figure 14: **Real-time autonomous topology morphing.** Evolution of learned routing probabilities on IBM Quantum hardware. Path A (blue) is initially preferred; upon failure detection at cycle 3 (red region), the optimizer transitions to Path B (orange), achieving complete rerouting by cycle 4.

based compilers cannot provide.

5 Conclusion

We have introduced a Differentiable Logical Programming (DLP) framework for quantum circuit design, a neuro-symbolic approach that recasts the NP-hard problem of circuit optimization into a continuous, gradient-based search. By representing a scaffold of candidate gates as learnable switches s (derived from structural logits λ) and optimizing them to satisfy differentiable logical axioms, our method provides a uniquely flexible tool for algorithm design. We have demonstrated that this single, unified framework can: (1) function as a “smarter” compiler discovering non-trivial optimizations from first principles; (2) perform de novo circuit discovery, such as the 12-gate 4-qubit QFT; (3) solve joint structural-parametric design problems; (4) scale to larger systems via Hierarchical Synthesis; and (5) perform real-time hardware-aware adaptation to temporal noise and failures, including a 59.3 percentage point fidelity improvement on the 133-qubit IBM Torino processor.

While currently focused on scaffold pruning within a fixed gate ordering, future work will extend this to full topological search by incorporating differentiable “Swap Networks.” The flexibility of this approach, built on standard automatic differentiation libraries, allows for a diverse range of tasks simply by composing different logical axioms, providing a potent methodological response to the challenges of the NISQ and early fault-tolerant eras.

5.1 Limitations and Scope: Fixed-Topology Optimization

It is important to distinguish between *topological discovery* (finding the optimal connectivity graph) and *scaffold pruning* (optimizing a selection from an ordered list). In this work, we focus on the latter. The DLP framework is currently constrained by the fixed ordering of the input scaffold S . If the optimal solution requires a permutation of gates not present in S , the model cannot discover it. However, this constraint is often intentional for the use case of *optimizing existing ansatzes*, where the ordering is dictated by a template. Future work will extend this to full topological search by incorporating differentiable “Swap Networks.”

The primary strength of this approach is its flexibility and ease of implementation. The same core model, built on standard `autograd` libraries like PyTorch, can solve this diverse range of tasks simply by composing different logical axioms in the loss function.

5.2 Data and Code Availability

The source code and data supporting the findings of this study are available from the corresponding author upon reasonable request. Scripts for reproducing the experiments will be made publicly available upon publication.

Acknowledgments

This work was supported by the Director of the Office of Science of the U.S. Department of Energy under Contract No. DE-AC02-05CH11231.

References

- [1] Michael A. Nielsen and Isaac L. Chuang. “Quantum computation and quantum information”. *Cambridge University Press*. Cambridge (2010). 10th anniversary edition.
- [2] Sam McArdle, Suguru Endo, Alán Aspuru-Guzik, Simon C. Benjamin, and Xiao Yuan. “Quantum computational chemistry”. *Reviews of Modern Physics* **92**, 015003 (2020).
- [3] Yudong Cao, Jonathan Romero, Jonathan P. Olson, Matthias Degroote, Peter D. Johnson, M. Kieferová, Ian D. Kivlichan, Tim

Menke, Borja Peropadre, Nicolas P. D. Sawaya, Sukin Sim, Libor Veis, and Alán Aspuru-Guzik. “Quantum chemistry in the age of quantum computing”. *Chemical Reviews* **119**, 10856–10915 (2019).

[4] Román Orús, Samuel Mugel, and Enrique Lizaso. “Quantum computing for finance: Overview and prospects”. *Reviews in Physics* **4**, 100028 (2019).

[5] Francesco Bova, Avi Goldfarb, and Roger G. Melko. “Commercial applications of quantum computing”. *EPJ Quantum Technology* **8**, 2 (2021).

[6] John Preskill. “Quantum computing in the NISQ era and beyond”. *Quantum* **2**, 79 (2018).

[7] Alberto Peruzzo, Jarrod R. McClean, Peter Shadbolt, Man-Hong Yung, Xiao-Qi Zhou, Peter J. Love, Alán Aspuru-Guzik, and Jeremy L. O’Brien. “A variational eigenvalue solver on a photonic quantum processor”. *Nature Communications* **5**, 4213 (2014).

[8] Edward Farhi, Jeffrey Goldstone, and Sam Gutmann. “A quantum approximate optimization algorithm” (2014). [arXiv:1411.4028](https://arxiv.org/abs/1411.4028).

[9] Jarrod R. McClean, Sergio Boixo, Vadim N. Smelyanskiy, Ryan Babbush, and Hartmut Neven. “Barren plateaus in quantum neural network training landscapes”. *Nature Communications* **9**, 4812 (2018).

[10] Harper R. Grimsley, Sophia E. Economou, Edwin Barnes, and Nicholas J. Mayhall. “An adaptive variational algorithm for exact molecular simulations on a quantum computer”. *Nature Communications* **10**, 3007 (2019).

[11] Seyon Sivarajah, Silas Dilkes, Alexander Cowtan, Will Simmons, Alec Edgington, and Ross Duncan. “ $t|ket\rangle$: a retargetable compiler for nisq devices”. *Quantum Science and Technology* **6**, 014003 (2020).

[12] Martin Lukac and Marek Perkowski. “Evolving quantum circuits using genetic algorithm”. In Proceedings of the 2002 NASA/DoD Conference on Evolvable Hardware. Pages 177–185. IEEE (2002).

[13] Matthew Amy, Dmitri Maslov, Michele Mosca, and Martin Roetteler. “A meet-in-the-middle algorithm for fast synthesis of depth-optimal quantum circuits”. *Trans. Comp.-Aided Des. Integ. Cir. Sys.* **32**, 818–830 (2013).

[14] Giulia Meuli, Mathias Soeken, and Giovanni De Micheli. “SAT-based CNOT, T quantum circuit synthesis”. In Reversible Computation (RC 2019). Volume 11497 of *Lecture Notes in Computer Science*, pages 175–188. Springer (2019).

[15] Shi-Xin Zhang, Chang-Yu Hsieh, Shengyu Zhang, and Hong Yao. “Differentiable quantum architecture search”. *Quantum Science and Technology* **7**, 045023 (2022).

[16] Wenjie Wu, Ge Yan, Xudong Lu, Kaisen Pan, and Junchi Yan. “Quantumdarts: Differentiable quantum architecture search for variational quantum algorithms”. In Proceedings of the 40th International Conference on Machine Learning. Volume 202 of *Proceedings of Machine Learning Research*, pages 37745–37764. PMLR (2023).

[17] Eric Jang, Shixiang Gu, and Ben Poole. “Categorical reparameterization with Gumbel-Softmax”. In International Conference on Learning Representations (ICLR). (2017). url: <https://openreview.net/forum?id=rkE3y85ee>.

[18] Chris J. Maddison, Andriy Mnih, and Yee Whye Teh. “The concrete distribution: A continuous relaxation of discrete random variables”. In International Conference on Learning Representations (ICLR). (2017). url: <https://openreview.net/forum?id=S1jE5L5gl>.

[19] Ryan Riegel, Alexander Gray, Francois Luus, Naweed Khan, Ndivhuwo Makondo, Ismail Yunus Akhalwaya, Haifeng Qian, Ronald Fagin, Francisco Barahona, Udit Sharma, Shajith Iqbal, Hima Karanam, Sumit Neelam, Ankita Likhiani, and Santosh Srivastava. “Logical neural networks” (2020). [arXiv:2006.13155](https://arxiv.org/abs/2006.13155).

[20] Hanxiao Liu, Karen Simonyan, and Yiming Yang. “DARTS: Differentiable architecture search” (2018). [arXiv:1806.09055](https://arxiv.org/abs/1806.09055).

[21] Ryan Babbush, Robbie King, Sergio Boixo, William Huggins, Tanuj Khattar, Guang Hao Low, Jarrod R McClean, Thomas O'Brien, and Nicholas C Rubin. “The grand challenge of quantum applications” (2025).

Additional Differentiable Axioms

Here we provide the mathematical forms for additional differentiable predicates \mathcal{T} and their corresponding loss terms \mathcal{L} that supplement the core axioms defined in Section 2.2.

Entanglement:

Used for de novo discovery of entangled states.

- **Predicate \mathcal{T}_{ent} :** Based on the Von Neumann entropy $S(\rho_A)$ of the reduced density matrix ρ_A for a bipartite split $A|B$.

$$\mathcal{T}_{\text{ent}}(U) = 1 - \exp(-kS(\rho_A(U))), \quad (23)$$

where $S(\rho_A) = -\text{Tr}(\rho_A \log_2 \rho_A)$ and k is a scaling factor.

- **Contradiction \mathcal{L}_{ent} :**

$$\mathcal{L}_{\text{ent}} = 1 - \mathcal{T}_{\text{ent}} = \exp(-kS(\rho_A)). \quad (24)$$

This loss term is ≈ 1 for separable states ($S = 0$) and $\rightarrow 0$ for maximally entangled states.

Robustness (Noise):

Used for multi-objective, noise-aware optimization.

- **Predicate E_{noisy} :** The average energy under a set of error channels $\mathcal{N} = \{N_j\}$, representing a noise model.

$$E_{\text{noisy}} = \frac{1}{|\mathcal{N}|} \sum_{N_j \in \mathcal{N}} \langle \psi | N_j^\dagger H N_j | \psi \rangle, \quad (25)$$

where $|\psi\rangle = U|0\rangle$.

- **Contradiction \mathcal{L}_{rob} :**

$$\mathcal{L}_{\text{rob}} = E_{\text{noisy}}. \quad (26)$$

This loss term is used in a multi-objective function, e.g., $\mathcal{L}_{\text{total}} = w_E \mathcal{L}_{\text{energy}} + w_R \mathcal{L}_{\text{rob}} + w_S \mathcal{L}_{\text{simp}}$.

Supplementary Experiments

S1: Robust VQE Ansatz Discovery with Annealing Curriculum

We applied the DLP framework to the nontrivial problem of finding the ground state for a 4-qubit 1D Ising model. This task is a common benchmark for Variational Quantum Eigensolvers (VQE) because the energy landscape contains a local minimum at $E = -4.0$ (a simple product state) that can trap gradient-based optimizers, preventing them from reaching the entangled ground state at $E \approx -4.73$. Our goal was to show that the framework can search this energy landscape and identify a simpler, noise-aware ansatz structure by pruning unnecessary gates from a generic hardware-efficient template.

The experiment utilized a scaffold composed of a standard hardware-efficient ansatz (HEA) layer, including parameterized $R_y(\theta)$ and $R_z(\phi)$ rotation gates and a chain of entangling $CNOT$ operations. To overcome the local minima problem, we employed the *Annealing Curriculum* strategy (Section 3.8). Instead of optimizing for the full Hamiltonian H immediately, we trained the model on a time-dependent Hamiltonian $H(t)$, where the interaction term J was slowly ramped from 0 to 1.0 over 8,000 epochs, see Figure 15 (c).

To further test robustness, we injected Gaussian noise ($\sigma = 0.1$) into the energy evaluation at every step. The optimization was driven by a composite loss function $\mathcal{L} = \mathcal{L}_{\text{energy}} + w_{\text{simp}}\mathcal{L}_{\text{simp}}$, which balanced the minimization of energy with a penalty for circuit complexity.

Results. As the annealing schedule progressed (epochs 0–8000), the system successfully escaped the $E = -4.0$ trap, converging to an energy of $E \approx -4.83$, which fluctuates around the theoretical ground state of -4.73 due to the injected noise. The structural learning (Fig. 15 (c)) reveals a physically intuitive result: the optimizer systematically pruned the R_z gates (driving their probabilities $s_i \rightarrow 0$) while retaining the R_y and $CNOT$ gates. This indicates the model correctly identified that for this real-valued Hamiltonian, Z -rotations were redundant, thereby autonomously simplifying the ansatz to its most efficient form without human intervention.

S2: QAOA Depth Discovery

While the main text focuses on circuit discovery and pruning in fixed scaffolds, this experiment isolates the framework’s ability to tune a discrete hyperparameter: circuit depth.

We tasked the model with finding the minimal QAOA (Quantum Approximate Optimization Algorithm) depth for a 4-node MaxCut instance, initializing a scaffold with $p_{\text{max}} = 3$ layers,

$$S = [U_C(\gamma_1), U_B(\beta_1), \dots, U_C(\gamma_3), U_B(\beta_3)].$$

Using a Two-Phase Curriculum: (1) we first optimized angles for energy with $w_{\text{simp}} = 0$, and then (2) applied simplicity pressure with $w_{\text{simp}} > 0$ to encourage pruning. The optimizer converged to $s_i \approx 0$ for the final ($p = 3$) layer, indicating that a reduced depth of $p = 2$ is sufficient for this problem.

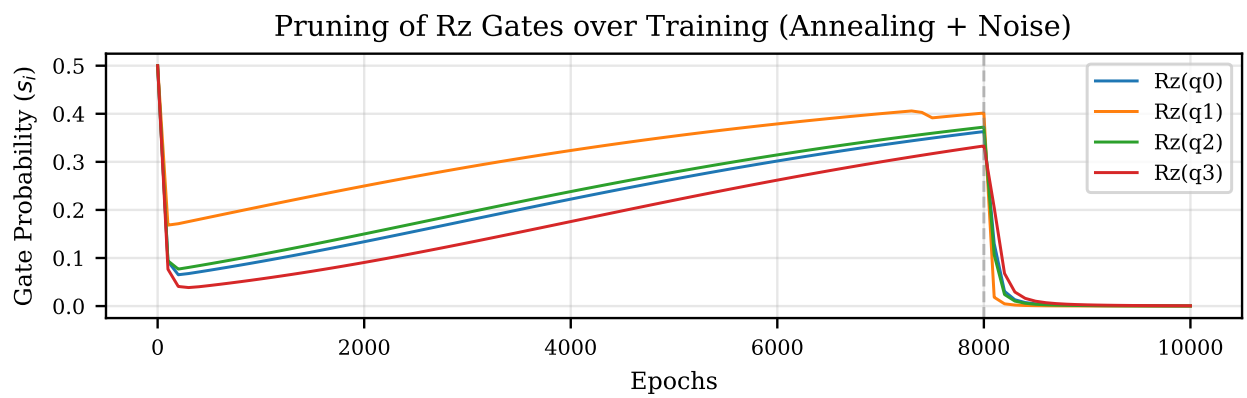
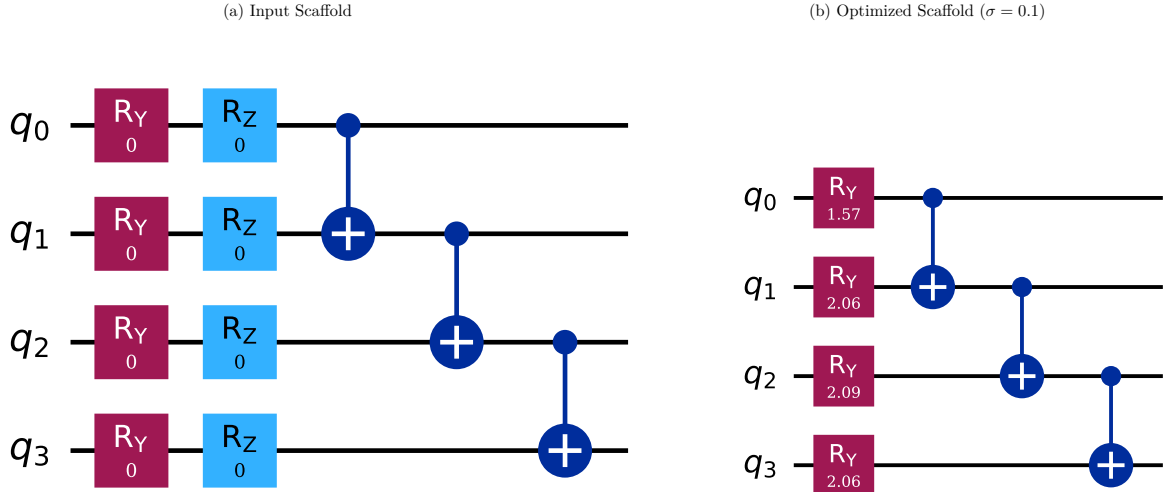


Figure 15: **VQE Discovery Results.** (a) The input scaffold represents a standard, over-parameterized ansatz. (b) The final circuit structure autonomously discovered by the model. Note that the R_z gates have been removed, leaving a minimal structure of R_y rotations and entangling $CNOTs$. (c) The evolution of the gate switch probabilities (s_i) for the R_z gates. As the curriculum introduces the interaction term J (epochs 0 – 8000) and the simplicity weight w_{simp} increases (epoch 8000+), the model decisively prunes these redundant operations, converging to a sparse topology while maintaining the ground state energy.